Design and Analysis of a Miniaturized-Metamaterial-Based Monopole Antenna for Ultra-Wide Band Wireless Communication System Using Machine Learning

Shadrack Naminde Ndete
Department of Electrical & Electronics Engineering, Pan African University Institute for Basic Sciences, Technology, and Innovation (PAUSTI), Juja, Kenya
shadracknaminde@gmail.com (corresponding author)

Franklin Muriuki Manene
Department of Electrical and Electronics Engineering, Dedan Kimathi University of Technology, Nyeri, Kenya
franklin.manene@dkuat.ac.ke

Robert Macharia Maina
Department of Telecommunication and Information Engineering, Jomo Kenyatta University of Agriculture and Technology (JKUAT), Juja, Kenya
rmmaina@jkuat.ac.ke

Received: 28 February 2025 | Revised: 4 April 2025 and 15 April 2025 | Accepted: 19 April 2025

 DOI: https://doi.org/10.48084/etasr.10710

ABSTRACT

This research presents a miniaturized microstrip Ultra-Wideband (UWB) antenna based on double square ring Metamaterial (MTM) for modern wireless communication devices. The MTM unit cells are placed on the back of the antenna to help improve antenna parameters (i.e., bandwidth, gain, radiation pattern, and efficiency). The antenna is based on an FR-4 substrate with a thickness of 1.5 mm, a relative permittivity of 4.4, and a dielectric loss tangent of 0.02. To achieve a solution in the frequency domain, simulations were performed using Ansys High-Frequency Structure Simulator (HFSS) software, an electromagnetic wave simulator based on a Finite Element Method (FEM)). Furthermore, a feeder with a characteristic impedance of 50 Ω has been applied. To address the computational time challenges associated with electromagnetic simulators like HFSS, Machine Learning (ML) in the form of an Artificial Neural Network (ANN) has been employed to optimize the antenna prior to the implementation of the MTM structure. The antenna's overall surface area is 24 × 12 mm^2, with an absolute bandwidth of 15.53 GHz, ranging from 3.83 GHz to 19.36 GHz. The maximum efficiency and gain are 98.79 % and 4.72 dB, respectively. The UWB antenna demonstrates superior performance in comparison to the results reported in recent studies employing MTMs and ML principles for optimization.

Keywords-microstrip antenna; miniaturized; metamaterials; Artificial Neural Network (ANN); Ultra-Wideband (UWB)

I. INTRODUCTION

Ultra-Wideband (UWB) technology has emerged as a pivotal innovation in wireless communication, offering significant advantages such as high data rate transmissions, low power consumption, and resilience to multipath interference. Approved by the Federal Communications Commission (FCC) in 2002, the UWB spectrum (3.1–10.6 GHz) has prompted extensive research and development in high-bandwidth and short-range communication systems [1, 2]. Microstrip patch antennas have gained prominence among various antenna types due to their low profile, lightweight design, and ease of integration with microwave circuits [3]. These antennas, consisting of a dielectric substrate sandwiched between a metallic patch and a ground plane, are preferred for their cost-effectiveness and simplicity in fabrication. However, conventional patch antennas face drawbacks, including narrow bandwidth, low gain, and limited efficiency [4, 5]. Overcoming these challenges has driven research into novel designs and

techniques, including introducing slotted ground planes, Defected Ground Structures (DGS), and innovative feedline methodologies.

The advent of Metamaterial (MTM) engineered structures with properties like negative permittivity and permeability has further revolutionized antenna design. MTM-based antennas have remarkably improved bandwidth, gain, and radiation efficiency [6]. The incorporation of features such as Split Ring Resonators (SRRs) and Capacitance-Loaded Strips (CLS) into MTM antennas has been demonstrated to yield performance enhancements that surpass traditional designs [7-9]. These structures have shown potential for UWB applications, addressing the challenges of compactness, efficiency, and performance within the FCC-defined spectrum.

Another critical consideration in modern antenna design is the integration of Machine Learning (ML) techniques to streamline development processes. High-frequency Electromagnetic simulations, while accurate, are computationally intensive and time-consuming [10]. ML models, such as Artificial Neural Networks (ANNs), offer a promising alternative for the modeling and optimization of complex antenna designs [11]. By learning the underlying relationships between geometric parameters and performance metrics, ML-based approaches can significantly reduce the iterative simulation burden and accelerate the design cycle [12, 13]. Recent studies have demonstrated the efficacy of ML in predicting parameters such as return loss, gain, and radiation patterns, thereby facilitating the design of efficient and innovative antenna structures.

This study presents the design and analysis of a miniature MTM-based monopole antenna for UWB wireless communication systems. The proposed design leverages the properties of MTMs and the predictive capabilities of ML to achieve enhanced bandwidth, gain, and compactness. The antenna under consideration incorporates double negative MTM on the bottom substrate and is optimized using ML algorithms to predict and refine its performance.

II. MATERIALS AND METHODS

A. Unit Cell Design

Geometrically, the unit cell comprises two double square copper string patches of 0.035 mm thickness, as illustrated in Figure 1.

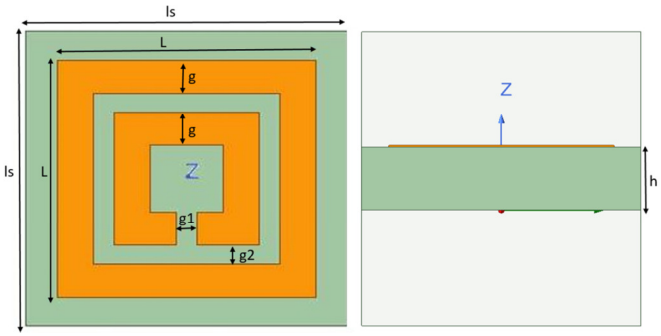

Fig. 1. 2D view of the MTM unit cell.

The patches are printed on a FR-4 substrate material with a thickness of 1.5 mm and a dielectric constant of 4.4. This geometrical arrangement introduces a magnetic field within the double square, which is responsible for negative permeability. The inner square stripe exhibits a rectangular gap (g1) with a width of 0.4 mm, introducing capacitance. Conversely, the outer square stripe is closed, leading to a reduction in series capacitance and an enhancement in coupling between the two square patch stripes. The design parameters of the proposed unit cell are as shown in Table I.

TABLE I. MTM UNIT CELL DESIGN PARAMETERS

Parameter	Dimensions (mm)
ls	6.2
L	5
g	0.7
g1	0.4
h	1.5
g2	0.4

B. Metamaterial Unit Cell Analysis

The MTM is placed between two waveguide ports along the positive and negative z-axis, facilitated by a waveport in Ansys High-Frequency Structure Simulator (HFSS). As the ideal magnetic conductor was placed perpendicular to the y-axis, the ideal electric conductor boundary was placed perpendicular to the x-axis. The operating frequency ranges from 2 to 20 GHz with an input normalized impedance of 50 Ω.

As indicated in [8, 14], the operation wavelength in the media should exceed the MTM unit cells. Figure 2 illustrates the S^{11} and S^{21} of the proposed SRR unit cell. The simulated S-parameters were exported to MATLAB for enhanced analysis and extraction of the electromagnetic properties.

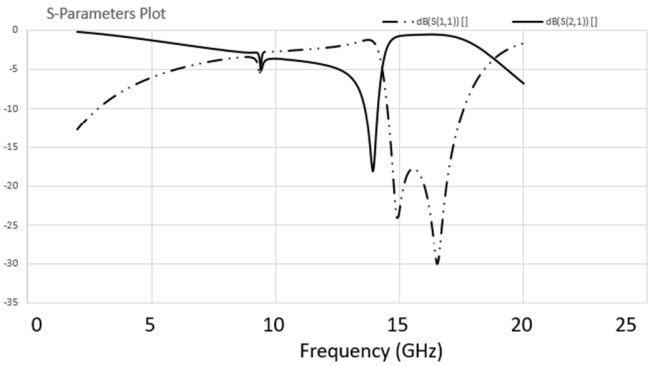

Fig. 2. MTM unit cell reflection and transmission coefficients.

A robust method is employed to verify the electromagnetic characteristics of the proposed SRR MTM [15, 16]. The robust method is well suited due to its ability to perform better in extreme cases, such as high or low frequencies, and better accuracies [17]. Equations (1) through (9) are employed to retrieve the electromagnetic parameters.

$$S^{11} = \left(\frac{R_{01}\left(1-e^{i2nk_0d}\right)}{1-R_{01}{}^2e^{i2nk_0d}}\right) \quad (1)$$

$$S^{21} = \left(\frac{(1-R_{01}{}^2)e^{ink_0d}}{1-R_{01}{}^2e^{i2nk_0d}}\right) \quad (2)$$

where $R_{01} = (z-1)/(z+1)$, d denotes the unit cell thickness, k_0 represents the wavenumber in free space, and z denotes the impedance.

$$\text{real}\,(z) \geq 0 \quad (3)$$

$$\text{imaginary}\,(n) \geq 0 \quad (4)$$

$$z = \pm\sqrt{\frac{(1+S_{11})^2-S_{21}{}^2}{(1-S_{11})^2-S_{21}{}^2}} \quad (5)$$

$$e^{ink_0d} = X \pm i\sqrt{1-X^2} \quad (6)$$

where $X = \frac{1}{2S_{21}(1-S_{11}{}^2+S_{21}{}^2)}$.

$$n = \frac{1}{k^0d}\times \left\{\left[\text{imaginary}\left[\ln e^{ink^0d}\right] + 2m\pi\right] - i\left[\text{real}\left[\ln e^{ink_0d}\right]\right]\right\} \quad (7)$$

where m is an integer value, and n is the refractive index.

$$\text{Permeability},\ \mu = nz \quad (8)$$

$$\text{Permittivity},\ \epsilon = \frac{n}{z} \quad (9)$$

The simulated real and imaginary parts of the effective permeability, permittivity, and refractive index for the unit cell are demonstrated in Figures 3 through 5.

The estimated MTM unit cell's negative permeability (μ) ranges from 2 GHz to 15.8462 GHz and from 19.3378 GHz to beyond 20 GHz, as shown in Figure 4. As illustrated in Figure 3, the suggested MTM unit cell's negative permittivity (ϵ) ranges from 2.1204 GHz to 10.4883 GHz and from 15.0033 GHz to 15.786 GHz. If a unit cell's permittivity and permeability stay negative at the same time, the refraction index will also be negative [18, 19]. As illustrated in Figure 5, a negative effective refractive index (n) is observed from 2.1204 GHz to 15.786 GHz. In the frequency range from 2.1204 GHz to 10.4883 GHz, the permeability, permittivity, and refractive index all exhibit negative values, indicating that the proposed unit cell possesses negative MTM properties.

C. Configuration of the Proposed Antenna

The design of the primary antenna (ANT1), as illustrated in Figure 6, consists of a circle and a rectangle, forming the radiating patch on top of a substrate. The substrate material of the antenna is a FR-4 epoxy substrate, with a relative dielectric constant (ϵ_r) of 4.4, a height of 1.5 mm, and 0.02 as the loss tangent ($\tan\delta$). Essentially, the ground plane has undergone further modification, entailing the removal of triangular extracts from the corners and the top edge, situated just below the feedline. The objective of the removal is to aid the antenna in achieving UWB characteristics. The optimal design parameters of ANT1 are illustrated in Table II, as determined by parametric analysis.

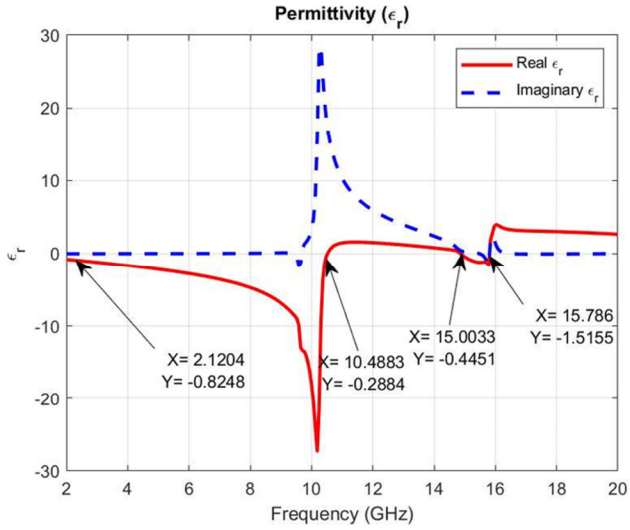

Fig. 3. MTM unit cell permittivity.

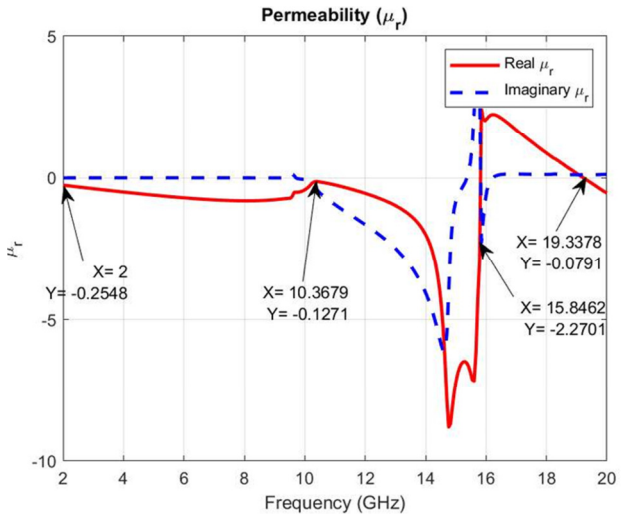

Fig. 4. MTM unit cell permeability.

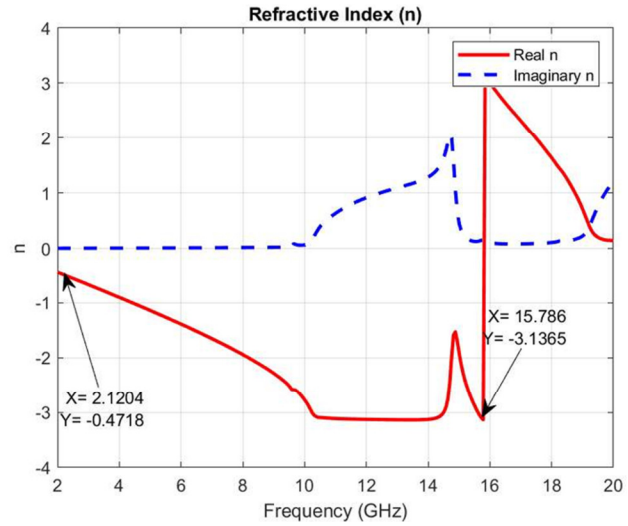

Fig. 5. MTM unit cell refractive index.

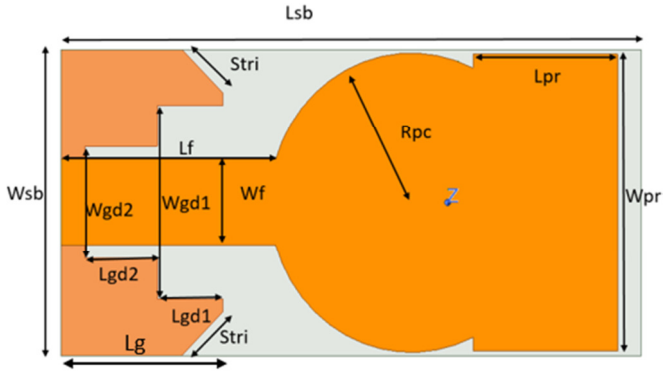

Fig. 6. Proposed antenna structure for ANT1.

TABLE II. DESIGN PARAMETERS OF THE PROPOSED ANTENNA (ANT1)

Parameter	Dimensions (mm)	Parameter	Dimensions (mm)
Lsb	24	Wf	3.5
Wsb	12	Stri	2.828
Rpc	5.7	Lf	10.025
Lpr	5	Lg	7
Wpr	12	Lgd2	3
Lgd1	3	Wgd2	4.4
Wgd1	6.7		

D. ANN Modelling

The objective of using ML at this stage is to ensure an optimal design (ANT2) prior to the introduction of MTMs. ANT2 is obtained from ANT1. For this stage, the MATLAB software was used to train the Multilayer Perceptron (MLP). The tool was used with feedforward backward propagation.

The present study utilized a total of 678 samples, incorporating 19 input features to generate 11 output features. The samples were generated from parametric analysis performed on ANT1 using HFSS software. Table III offers a comprehensive overview of the parametric analysis methodology employed to obtain the 678 samples. Each parameter was modified individually, while the remaining parameters remained constant. The parameter under observation was modified according to the steps provided. The start and end values were selected in such a way that they do not have ambiguous deformations for the antenna. The 11 geometric features are as follows: Lg, Lgd1, Wgd1, Lgd2, Wgd2, Wf, Rpc, Lpr, Wpr, Stri, and Lf. The output return loss values at the following frequency points are to be considered: 2 GHz, 3.05 GHz, 4.11 GHz, 5.17 GHz, 6.23 GHz, 7.29 GHz, 8.33 GHz, 9.41 GHz, 10.47 GHz, 11.52 GHz, 12.58 GHz, 13.64 GHz, 14.70 GHz, 15.76 GHz, 16.82 GHz, 17.88 GHz, 18.94 GHz, and 20 GHz, with the addition of the average gain, summing to 19 features. In HFSS, the geometric features are treated as inputs, as the return loss values and the average gain are outputs. This is reversed when using the neural network model where the 18 return loss values plus 1 gain value are fed into the model to generate the geometric values for the desired optimal antenna. Of the 678 samples collected, 70% are used to train the model, followed by 15% for model validation and 15% for testing.

TABLE III. START AND END VALUES FOR PARAMETRIC ANALYSIS ON GEOMETRIC PARAMETERS FOR ANT1

Parameter	Start	End	Step
Lg	5.7	7	0.025
Lgd1	0.3	5	0.094
Wgd1	5.7	10	0.05
Lgd2	0.3	3	0.005
Wgd2	2	6	0.05
Wf	3.2	3.8	0.01
Rpc	5.1	5.7	0.01
Lpr	1	7	0.1
Wpr	6	12	0.1
Stri	5	7	0.05
Lf	1.7	4.7	0.075

The ANN architecture used for the design and validation of the microstrip patch antennas is based on the hidden and output layers. The transfer functions used in this neural network architecture include the pure linear transfer function (purelin) applied to the hidden layer and the hyperbolic tangent sigmoid transfer function (tansig) applied to the output layer.

The neural network training process, implemented using MATLAB's nntraintool, employs the Levenberg-Marquardt training algorithm and uses Mean Squared Error (MSE) as the performance metric. During training, several key metrics are monitored to ensure proper convergence and model optimization. MSE represents the mean squared error between the predicted outputs and the target outputs. Initially, the MSE is high (33.1), but it decreases significantly during training to 0.00324, indicating improved model accuracy as training progresses. The gradient reflects the rate of change of the performance function with respect to the weights. As training progresses, the gradient decreases from 46.7 to 0.000743, indicating that the model is approaching convergence. The damping parameter, Mu, is a part of the Levenberg-Marquardt optimization and controls the step size during training. Initially set to 0.001, Mu decreases to 1.00e-05, indicating that the model is fine-tuning the weights as it nears convergence. Validation checks are utilized to monitor the performance of the model on a validation dataset. In this case, six validation checks were performed, ensuring that the model generalizes well without overfitting.

To determine the best number of neurons for the hidden layer, the MSE for different neurons was determined, as shown in Figure 7. The figure shows that 30 neurons give the lowest MSE value of 0.002512. The R-value of the regression indicates the correlation between the target and the output, with R-values closer to one suggesting a highly similar relationship. In an ideal scenario, the target and the outputs are the same. The MSE and R-values are calculated using the following equations [10].

$$MSE = \frac{1}{N}\sum_{i=1}^{N}(R_i - P_i)^2 \quad (10)$$

$$R = \sqrt{1 - \frac{\sum(R_i - P_i)^2}{\sum(R_i - R_m)^2}} \quad (11)$$

where N is the number of testing or training samples, P_i are the predicted output values, R_i are the target output values; R_m is the mean value of R_i.

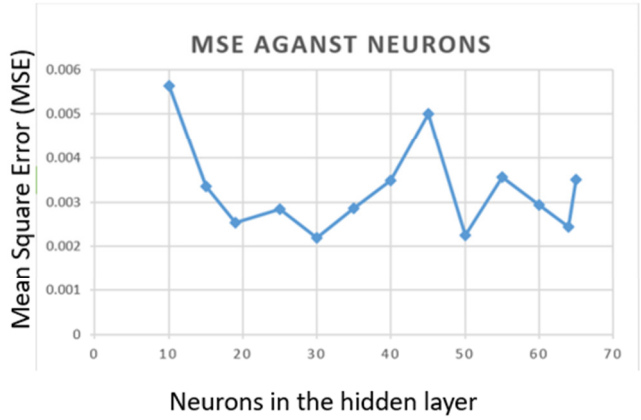

Fig. 7. Plot of MSE against several neurons.

The MSE value of the training approaches zero and was found to be 0.0043996, and R was found to be 0.99845. Considering the rest of the values, MSEs can be said to approach zero, while R values vary between 0 to 1 [10]. The training, validation, test results, and actual values are plotted against one another in Figure 8. The value of the training results is 99.845%. In general, a value between 80% and 90% is good for training in ANN applications. In this study, the estimation percentage of the data equals 99.831%.

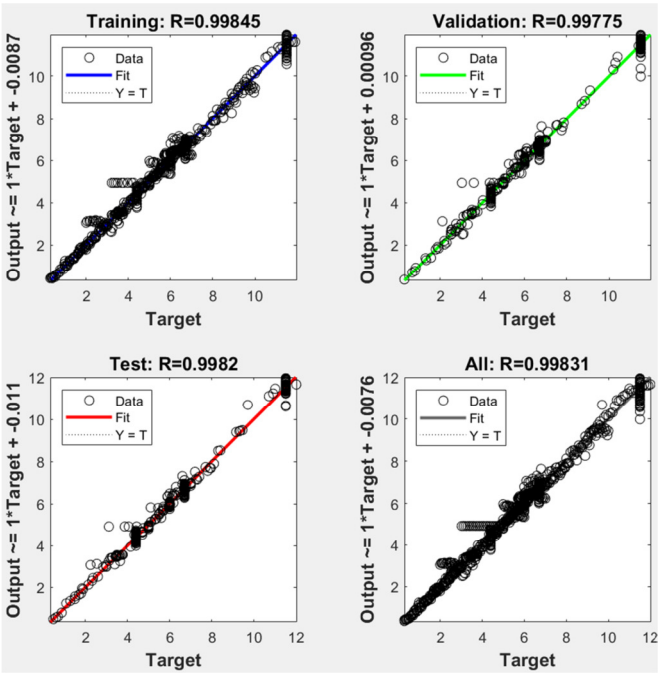

Fig. 8. Regression graphs of S^{11} and gain versus geometrical parameters.

The trained model provides the best geometric values of the optimum antenna, as shown in Table IV. When these values are inserted and simulated in the HFSS antenna design, a wide bandwidth is obtained for ANT2. This is an improvement from what was obtained in the initial design (ANT1) with an increase of 7.03 GHz.

TABLE IV. OPTIMIZED PARAMETERS OF THE PROPOSED ANTENNA (ANT2)

Parameter	Dimensions (mm)	Parameter	Dimensions (mm)
Lsb	24	Wf	3.36
Wsb	12	Stri	2.4
Rpc	5.85	Lf	8.9
Lpr	5.98	Lg	7.084
Wpr	11.63	Lgd2	3
Lgd1	2.709	Wgd2	4.3976
Wgd1	7.597		

E. Metamaterial based Antenna

The optimal position of the MTM was found to be as demonstrated in Figure 9 using parametric analysis. The initial step in performing a parametric analysis is to initiate the ANT2 setup in HFSS, where two new variables, designated as $LO and $LP, are introduced. These values are determined in such a way that their addition or subtraction alters the general position of the MTMs, causing them to move on either side of the x-axis. The MTMs are not supposed to make contact with the ground or extend beyond the substrate on the positive side of the x-axis, meaning their movement is bound.

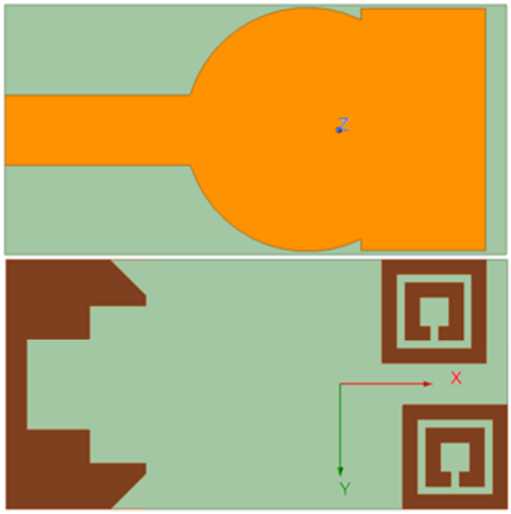

Fig. 9. Proposed antenna structure with 2 MTM unit cells.

The parametric analysis was conducted on a single MTM unit cell prior to the addition of the second cell; therefore, the cells are not on the same line, as illustrated in Figure 9. The procedure can be summarized as follows:

1. The antenna model (ANT2) is opened in HFSS.
2. The parameters to be analyzed ($LO and $LP) are added on 'Project', i.e. Project > Project variables > Add > Add property.
3. Now the parameters/variables are incorporated into the MTM unit cells specifically to impact the x-axis movement, e.g. -1 mm + $LP, -6 mm, 0 mm in this format 'x, y, z' axes.

4. Configure the parametric analysis: This is made possible by going to the Optimetrics, i.e. Optimetrics > Add parametric setup > Add > Variable ($LO) > Linear step > Define the start value, end value and the steps.
5. Start the simulation: Click 'Analyze All' to run the parametric sweep. This can be found by right clicking on the HFSS design just below the project name. HFSS will automatically solve the design for each combination of parameter values.

The return loss plot illustrated in Figure 10 (ANT3) shows the final optimized antenna.

III. RESULTS AND DISCUSSION

This section presents the antenna parameters of return loss, bandwidth, gain, radiation pattern, and efficiency of the three antennas (ANT1, ANT2, and ANT3).

A. Return Loss

This is a measure of the electrical power delivered into an antenna from a feed point [20-24]. It indicates good impedance matching when the values of S^{11} are negative, and for the antenna to perform better in real-time applications, these values should be less than -10 dB [25]. Good impedance matching means less reflected power and maximum power delivered into the antenna. Figure 10 shows the return loss plots for the three antennas described in this analysis: the reference antenna, ANT1, which exhibits a first resonance near 4.2 GHz, a second resonance near 10.26 GHz, and a third and final resonance near 17.44 GHZ, leading to return losses of -19.178 dB, -20.66 dB, and -11.68 dB, respectively. ANT2 was designed using the ANN, and had five resonance points: 4.3 GHz, 7 GHz, 11.34 GHz, and 15.85 GHz with return losses of -18.88 dB, -15.29 dB, -28.44 dB, -19.79 dB, and 17.88 GHz with a return loss of -25.63 dB. The proposed antenna (ANT3) has the same resonant frequencies plus a lower return loss of -36.24 dB at 17.7 GHz. Other resonant frequencies are 4.3 GHz, 7.05 GHz, 10.48 GHz, 10.93 GHz, and 11.79 GHz with return loss of -19.5 dB, -14.75 dB, -28.07 dB, -27.67 dB, and -33.6 dB, respectively. The improvements in ANT3 demonstrate the effect of the MTM on the antenna resonant frequencies.

B. Bandwidth

The bandwidth of an antenna is where it can effectively operate in terms of receiving and transmitting power. Return loss curves are used to determine the antenna bandwidth. This means that the bands operating below the -10 dB line are considered to be the antenna bandwidth. As illustrated in Figure 10, ANT1 exhibits two multi-bands, 3.8 GHz to 12.38 GHz and 16.08 GHz to 18.9 GHz, with an impedance bandwidth of 8.58 GHz and 2.82 GHz, respectively. The second antenna (ANT2) can achieve a wide bandwidth from 3.85 GHz to 19.46 GHz with an impedance bandwidth of 15.61 GHz. The resonant frequency with the lowest return loss for this antenna is 11.34 GHz. In addition to the highest resonant frequencies, the proposed antenna has an ultra-wide bandwidth from 3.83 GHz to 19.36 GHz, with an impedance bandwidth of 15.53 GHz.

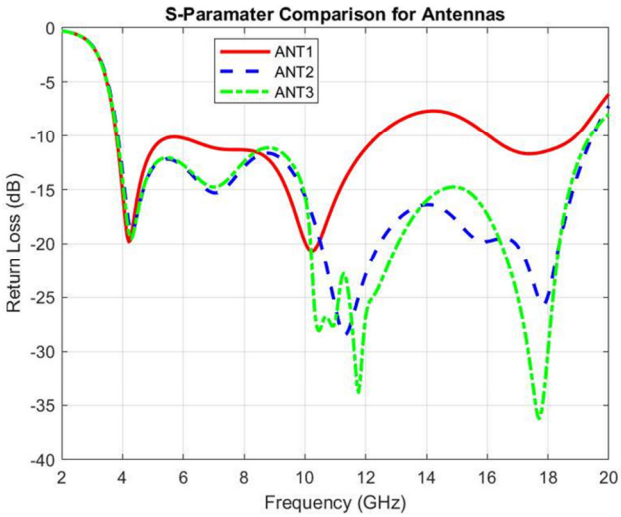

Fig. 10. Reflection coefficients for the three antennas (ANT1, ANT2, and ANT3).

C. Radiation Pattern

The radiation pattern is a critical parameter for evaluating an antenna's performance, as the primary function of an antenna is to radiate. Figure 11 presents simulated 3D views of the far-field radiation patterns for the three antennas at 6.85 GHz. The colors red and blue indicate the strongest and weakest radiation, respectively. The radiation pattern indicates omnidirectional radiation, with the proposed antenna (ANT3) having a maximum power of 21.27 dB compared to ANT2 and ANT1 with 21.25 dB and 20.99 dB, respectively. This indicates a significant advantage in ultra-wideband communication systems.

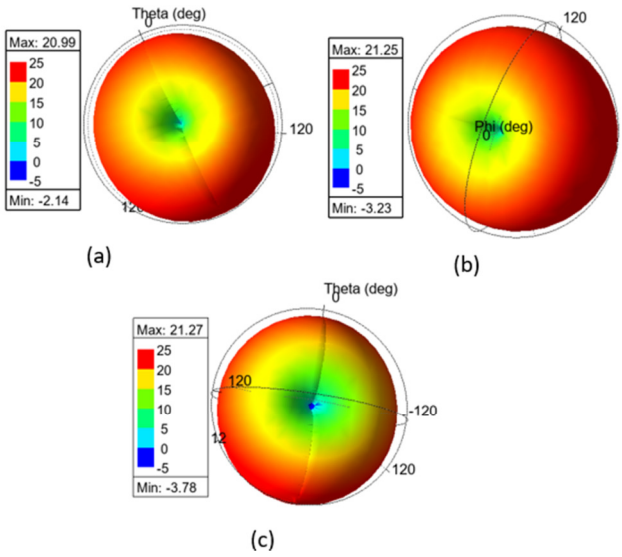

Fig. 11. 3D radiation pattern at 6.85GHz: (a) ANT1, (b) ANT2, (c) ANT3.

D. Gain

Gain is a factor that describes how directional the antenna is; a low gain antenna means that the antenna can radiate in all

directions, as opposed to a high gain antenna that is specific to a particular direction. As shown in Figure 12 and Table V, ANT1 has a peak and average gain of 6.78 dB and 4.63 dB, respectively. At the same time, ANT2 has a peak and average gain of 6.83 dB and 4.35 dB, respectively, whereas ANT3 has a peak and average gain of 6.88 dB and 4.72 dB, respectively. It is worth noting the effect of the MTM on the gain of the antenna, increasing it by 0.37 dB (average gain) over ANT2 and 0.09 dB over ANT1. The E-plane and H-plane plots for the three antennas (ANT1, ANT2 and ANT3) at a frequency of 6.5 GHz are shown in Figure 13 to 15, respectively. It is observed that ANT3 has the highest gain among the three antennas of 3.661 dB in the E-plane and 3.3416 dB in the H-plane.

E. Efficiency

Antenna efficiency is evaluated as the ratio of energy input to energy output. A highly efficient antenna will radiate most of the power applied to its input, whereas a less efficient antenna will lose some of its power due to internal losses or impedance mismatch-induced reflection. The efficiency is identical for transmitting and receiving antennas, and it is more intuitive to consider efficiency the as the proportion of energy radiated compared to the energy supplied. It can be expressed as $\eta = \text{Energy radiated}/\text{Energy input}$.

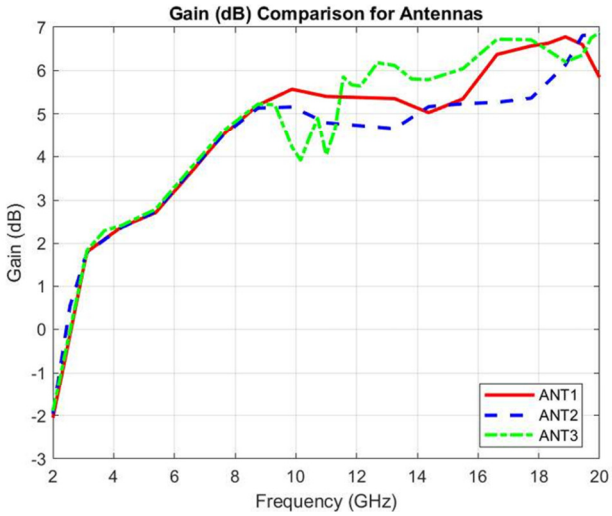

Fig. 12. Gain plots for the three antennas (ANT1, ANT2 and ANT3).

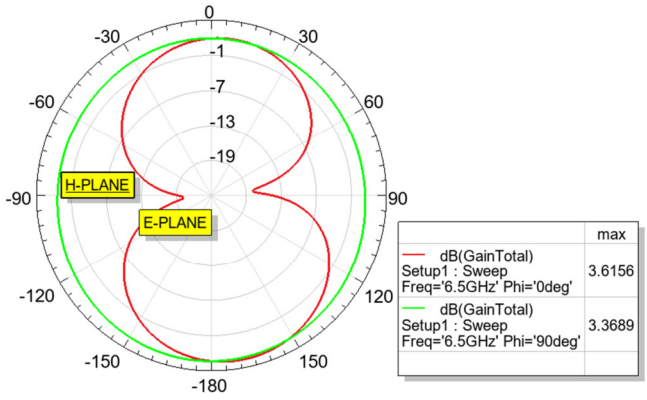

Fig. 13. E-plane and H-plane gain plots for ANT1 at 6.5 GHz.

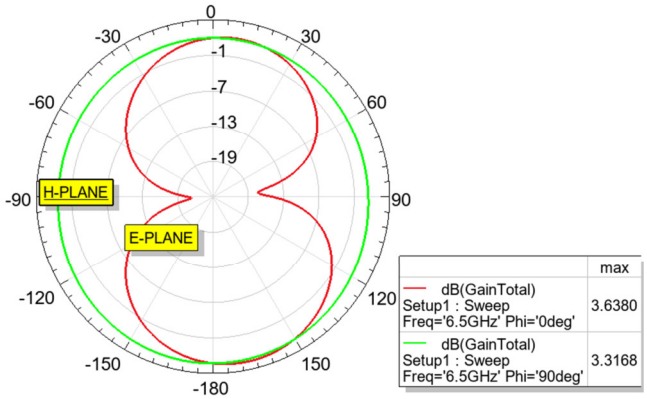

Fig. 14. E-plane and H-plane gain plots for ANT2 at 6.5 GHz.

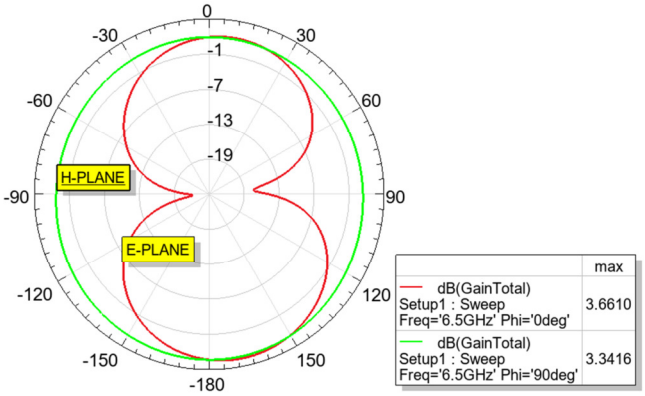

Fig. 15. E-plane and H-plane gain plots for ANT3 at 6.5 GHz.

Figure 16 shows the radiation efficiency curves for the three antennas. What is common is a radiation efficiency of more than 85% across the entire band. However, ANT3 has the highest value of maximum efficiency (98.8 %). It clearly shows that the proposed antenna efficiently radiates the power generated at the input.

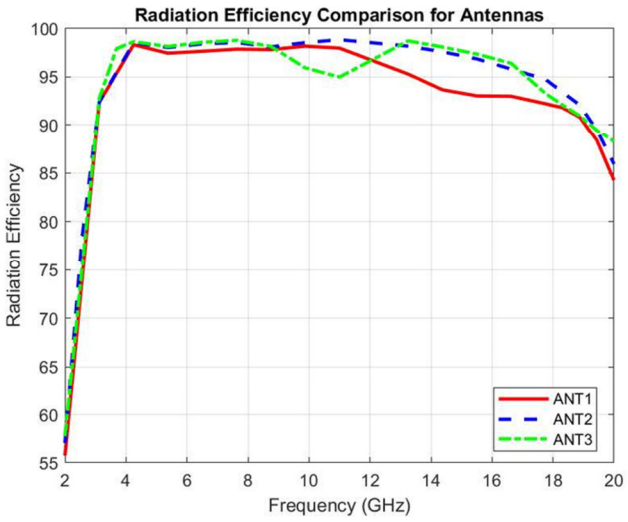

Fig. 16. Radiation efficiency and gain plots of the three antennas (ANT1, ANT2 and ANT3).

Table V shows a summary of the performance of the three antennas, i.e., ANT1, ANT2, and ANT3.

TABLE V. COMPARISON OF ANT1, ANT2, AND ANT3

Parameter	ANT1	ANT2	ANT3
Bandwidth (GHz)	3.8 - 12.38, 16.08 - 18.9	3.85 - 19.46	3.83 - 19.36
Fractional bandwidth (%)	106, 16.1	134	133.93
Average gain (dB)	4.6279	4.35	4.72
Peak gain (dB)	6.777	6.8267	6.88
Max radiation efficiency (%)	98.33	98.85	98.79

IV. COMPARISON OF THE PROPOSED WORK WITH RECENT STUDIES

In order to demonstrate the advantages of the proposed antenna, the performance of related antennas in the literature are studied to avoid impartiality in the analysis. Table VI presents a comparative study between the proposed ultra-compact UWB antenna and previously published designs in terms of size, bandwidth, peak gain and efficiency. While previous studies have employed various design techniques such as slot loading [2, 26], MTM unit cells [18], and defected ground structures [27], the proposed work leverages an MTM-based design with negative index characteristics, which is optimized using ML (ANN). Compared to previous designs, the proposed antenna is among the smallest, with overall dimensions of 24 × 12 × 1.5 mm³. The closest in size is the design in [2] (13 × 27.2 × 1.5 mm³), but it offers a significantly lower bandwidth (2.8382–9.0682 GHz) and peak gain (2.6 dB). Most other designs are notably larger, such as [27] (30 × 20 × 0.8 mm³) and [28] (30.8 × 27.6 × 0.8 mm³), yet they do not achieve a comparable gain or efficiency. The proposed antenna exhibits an exceptionally wideband response, covering 3.83–19.36 GHz with an overall bandwidth of 133.93%. This significantly surpasses designs such as [1] (3.581–3.935 GHz) and [26] (3–11 GHz). The closest competing design in terms of bandwidth is [27] (3.15–22.85 GHz), but it has a much lower gain (4.4599 dB) and efficiency (95.779%). By achieving a peak gain of 6.88 dB, the proposed antenna provides a stronger signal compared to all listed designs, surpassing even the best-performing [18] (6.12 dB). Additionally, it achieves an exceptional efficiency of 98.79%, which is among the highest reported, slightly exceeding [20] (98.44%). Most of the other antennas, such as [28] (92.28%) and [1] (82%), demonstrate lower efficiency, highlighting the superior design of the proposed model.

TABLE VI. COMPARISON OF PRESENT WORK WITH PREVIOUSLY PUBLISHED WORK

Ref.	Antenna size (mm^3)	Bandwidth (GHz)	Peak gain (dB)	Efficiency (%)
[1]	27×25×1.5	3.581–3.935	4.7	82
[2]	13×27.2×1.5	2.8382–9.0682	2.6	
[18]	14.5×22×1.6	3.08–14.1	6.12	97
[20]	21×27×1.6	3.16–14.36	4.1	98.44
[26]	25×22×1.6	3–11	4.1	85
[27]	30×20×0.8	3.15–22.85	4.4599	95.779
[28]	30.8×27.6×0.8	3.5–14.5	2.8	92.28
Proposed	24×12×1.5	3.83–19.36	6.88	98.79

V. CONCLUSION

This work presents a miniaturized Ultra-Wideband (UWB) microstrip patch antenna based on Metamaterial (MTM) with negative index characteristics, which is designed using Ansys High-Frequency Structure Simulator (HFSS) and successfully optimized using Machine Learning (ML), specifically Artificial Neural Network (ANN). This simulated negative index MTM antenna gives an overall bandwidth of 133.93%. The designed antenna, operating from 3.8 GHz to 19.3 GHz, exhibits UWB characteristics, making it suitable for various wireless applications. Its high efficiency (98.79%) and peak gain (6.88 dB) enable its use in UWB communications (3.1–10.6 GHz), 5G sub-6 GHz and mmWave networks, radar and imaging systems (X-band, Ku-band), satellite communications, and RF energy harvesting. Its compact size (24 × 12 × 1.5 mm) allows integration into miniaturized and wearable devices, enhancing portability and versatility. Given these attributes, the antenna demonstrates strong potential for next-generation wireless systems, facilitating high-speed data transmission, precise sensing, and efficient energy transfer. The proposed antenna exhibited excellent radiation patterns, operating as an omnidirectional at the UWB center frequency. The fabrication of the suggested antenna, as well as an assessment of the effectiveness of the practical and simulated antennas, will be the main topics of future work.

ACKNOWLEDGMENT

This research has been made possible by the support from the African Union and directly through the Pan African University Institute for Basic Sciences, Technology, and Innovation (PAUSTI).

REFERENCES

[1] M. S. Jameel, Y. S. Mezaal, and D. C. Atilla, "Miniaturized Coplanar Waveguide-Fed UWB Antenna for Wireless Applications," *Symmetry*, vol. 15, no. 3, Mar. 2023, Art. no. 633, https://doi.org/10.3390/sym15030633.

[2] Y. S. Mezaal, K. Al-Majdi, A. Al-Hilalli, A. A. Al-Azzawi, and A. A. Almukhtar, "New miniature microstrip antenna for UWB wireless communications," *Proceedings of the Estonian Academy of Sciences*, vol. 71, no. 2, pp. 194–202, May 2022, https://doi.org/10.3176/proc.2022.2.06.

[3] M. F. Ahmed, A. Z. Md. T. Islam, and M. H. Kabir, "Design of a Ultra-Wideband Rectangular Patch Microstrip Antenna with Improved Bandwidth," *International Journal of Recent Engineering Science*, vol. 8, no. 5, pp. 6–12, Oct. 2021, https://doi.org/10.14445/23497157/IJRES-V8I5P102.

[4] J. Nourinia, C. Ghobadi, and B. Mohammadi, "Printed UWB Antennas: Design and Principle," in *Wideband, Multiband, and Smart Antenna Systems*, M. A. Matin, Ed. Cham, Switzerland: Springer International Publishing, 2021, pp. 39–93, https://doi.org/10.1007/978-3-030-74311-6_3.

[5] A. K. Nghaimesh and A. K. Jassim, "Triple-Band Circular Patch Microstrip Antenna for Wireless Communication," *Journal of Engineering and Sustainable Development*, vol. 28, no. 1, pp. 65–75, Jan. 2024, https://doi.org/10.31272/jeasd.28.1.5.

[6] N. A. Othman *et al.*, "Zero-Biasing Split Ring Resonator using Metamaterial Element for High Gain Superstrates Ultra-Wideband Antenna," *Journal of Advanced Research in Applied Sciences and Engineering Technology*, vol. 30, no. 1, pp. 321–330, Mar. 2023, https://doi.org/10.37934/araset.30.1.321330.

[7] M. Moniruzzaman *et al.*, "Gap coupled symmetric split ring resonator based near zero index ENG metamaterial for gain improvement of

monopole antenna," *Scientific Reports*, vol. 12, no. 1, May 2022, Art. no. 7406, https://doi.org/10.1038/s41598-022-11029-7.

[8] M. M. Islam, M. T. Islam, M. Samsuzzaman, M. R. I. Faruque, N. Misran, and M. F. Mansor, "A Miniaturized Antenna with Negative Index Metamaterial Based on Modified SRR and CLS Unit Cell for UWB Microwave Imaging Applications," *Materials*, vol. 8, no. 2, pp. 392–407, Feb. 2015, https://doi.org/10.3390/ma8020392.

[9] M. Alsharari, A. Armghan, and K. Aliqab, "Monopole Antenna Modeling and Optimization for 5G Communication System using Machine Learning," in *2023 International Wireless Communications and Mobile Computing*, Marrakesh, Morocco, 2023, pp. 390–393, https://doi.org/10.1109/IWCMC58020.2023.10183161.

[10] M. Mushaib, D. A. Kumar, and D. R. K. Singh, "Designing and Validation of Micro strip Patch Antenna Using Artificial Neural Networks," *International Journal of Advances in Engineering and Management*, vol. 6, no. 6, pp. 440–459, Jun. 2024, https://doi.org/10.35629/5252-0606440459.

[11] D. Sarkar, T. Khan, and R. H. Laskar, "Multi-parametric ANN modelling for interference rejection in UWB antennas," *International Journal of Electronics*, vol. 107, no. 12, pp. 2068–2083, Dec. 2020, https://doi.org/10.1080/00207217.2020.1756449.

[12] N. Sarker, P. Podder, M. R. H. Mondal, S. S. Shafin, and J. Kamruzzaman, "Applications of Machine Learning and Deep Learning in Antenna Design, Optimization, and Selection: A Review," *IEEE Access*, vol. 11, pp. 103890–103915, 2023, https://doi.org/10.1109/ACCESS.2023.3317371.

[13] M. Sagik *et al.*, "C-shaped split ring resonator type metamaterial antenna design using neural network," *Optical Engineering*, vol. 60, no. 4, Apr. 2021, Art. no. 047106, https://doi.org/10.1117/1.OE.60.4.047106.

[14] N. K. Majji, V. N. Madhavareddy, G. Immadi, N. Ambati, and S. M. Aovuthu, "Analysis of a Compact Electrically Small Antenna with SRR for RFID Applications," *Engineering, Technology & Applied Science Research*, vol. 14, no. 1, pp. 12457–12463, Feb. 2024, https://doi.org/10.48084/etasr.6418.

[15] N. E. H. Nasri, M. EL Ghzaoui, S. Das, B. Jackson, B. T. P. Madhav, and M. Fattah, "A square split ring resonator-based metamaterial integrated high gain 4×4 MIMO antenna with circular polarization for wideband 5G millimeter-wave applications," *Optical and Quantum Electronics*, vol. 56, no. 6, Apr. 2024, Art. no. 971, https://doi.org/10.1007/s11082-024-06914-6.

[16] N. A. Othman, M. A. Jamlos, W. A. Mustafa, and S. Z. Syed Idrus, "Simulation Study of Metamaterial Effect towards Ultra Wide Band Antenna," *IOP Conference Series: Materials Science and Engineering*, vol. 917, no. 1, Sep. 2020, Art. no. 012073, https://doi.org/10.1088/1757-899X/917/1/012073.

[17] S. S. Al-Bawri *et al.*, "Metamaterial Cell-Based Superstrate towards Bandwidth and Gain Enhancement of Quad-Band CPW-Fed Antenna for Wireless Applications," *Sensors*, vol. 20, no. 2, Jan. 2020, Art. no. 457, https://doi.org/10.3390/s20020457.

[18] S. S. Al-Bawri *et al.*, "Compact Ultra-Wideband Monopole Antenna Loaded with Metamaterial," *Sensors*, vol. 20, no. 3, Feb. 2020, Art. no. 796, https://doi.org/10.3390/s20030796.

[19] D. K. Somwanshi, "Review of Antenna Performance Based on Metamaterials," in *Metamaterial Technology and Intelligent Metasurfaces for Wireless Communication Systems*, S. Mehta and A. N. Abougreen, Eds. Hershey, PA, USA: IGI Global Scientific Publishing, 2023, pp. 36–63, https://doi.org/10.4018/978-1-6684-8287-2.ch002.

[20] M. S. Karoui, N. Ghariani, M. Lahiani, and H. Ghariani, "Bandwidth Enhancement of a Bell-shaped UWB Antenna for Indoor Localization Systems," *Engineering, Technology & Applied Science Research*, vol. 11, no. 1, pp. 6691–6695, Feb. 2021, https://doi.org/10.48084/etasr.3975.

[21] A. K. Singh, M. P. Abegaonkar, and S. K. Koul, *Metamaterials for Antenna Applications*, 1st ed. Boca Raton, FL, USA: CRC Press, 2021, https://doi.org/10.1201/9781003045885.

[22] E. Ahamed, M. R. I. Faruque, M. F. B. Mansor, and M. T. Islam, "Polarization-dependent tunneled metamaterial structure with enhanced fields properties for X-band application," *Results in Physics*, vol. 15, Dec. 2019, Art. no. 102530, https://doi.org/10.1016/j.rinp.2019.102530.

[23] S. K. Ibrahim *et al.*, "Compact metamaterial-based single/double-negative/near-zero index resonator for 5G sub-6 GHz wireless applications," *Scientific Reports*, vol. 14, no. 1, Jun. 2024, Art. no. 12834, https://doi.org/10.1038/s41598-024-63610-x.

[24] U. M. Lambert, U. K. Michael, and O. A. Bernard, "Ultra-wideband Metamaterial-based Rectangular Microstrip Antenna for Sub-6 GHz 5G and other Microwave Applications," *Journal of Engineering Research and Reports*, vol. 25, no. 7, pp. 1–10, Jul. 2023, https://doi.org/10.9734/jerr/2023/v25i7932.

[25] K. Y. Yazdandoost and R. Kohno, "Design and Analysis of an Antenna for Ultra-Wideband System," in *14th IST Mobile and Wireless Communications Summit*, Dresden, Germany, 2005.

[26] S. Ahmad *et al.*, "A Jug-Shaped CPW-Fed Ultra-Wideband Printed Monopole Antenna for Wireless Communications Networks," *Applied Sciences*, vol. 12, no. 2, Jan. 2022, Art. no. 821, https://doi.org/10.3390/app12020821.

[27] F. Ahmed, H. Kabir, and T. Islam, "Design of a compact patch antenna with bandwidth and efficiency improvement for UWB applications," *Multidisciplinary Science Journal*, vol. 5, no. 4, May 2023, Art. no. 2023030, https://doi.org/10.31893/multiscience.2023030.

[28] P. K. Sharma, D. Sharma, T. J. V. S. Rao, J. R. Szymański, M. Żurek-Mortka, and M. Sathiyanarayanan, "Design & implementation of a meta-material based ultra-wide band microstrip patch antenna for vehicular communication," *Microsystem Technologies*, vol. 31, no. 2, pp. 547–558, Feb. 2025, https://doi.org/10.1007/s00542-024-05831-8.